Mathematical Modelling of Entrained Flow Gasifier Using Partial Differential Equations

Imran Nazir Unar[1], Sumaira Yousuf Khan[2*], Attra Ali[3], Masroor Abro[1], Ghulamullah Maitlo[4]

[1]Department of Chemical Engineering, Mehran University of Engineering and Technology Jamshoro, Pakistan

[2]Department of Mathematics, Dawood University of Engineering and Technology Karachi, Pakistan

[3]Department of Mathematics, Institute of Business Management, Karachi Pakistan

[4]Department of Chemical Engineering, Dawood University of Engineering and Technology Karachi, Pakistan

*Corresponding Author: Sumaira Yousuf Khan

***Abstract**: In this research entrained flow gasifier is modeled through commercially available Computational Fluid Dynamics (CFD) software Ansys Fluent®14. The general continuity equation, energy equation, and Navier-Stoke fluid flow equations were solved using the CFD modeling approach. The mathematical modeling was done using differential partial equations. The turbulence was predicted using the standard k-ε turbulence model. Co-gasification of coal and biomass for syngas production is considered environmentally friendly. Numerous thermal conversion technologies have been used for the co-gasification of coal and biomass, but multiple opposite burner (MOB) gasifiers got more attention because of their higher efficiency during the gasification of low-grade coal and biomass. The MOB gasifiers are commonly used for coal and biomass gasification. However, MOB gasifiers were not used with the combination of low-grade coal and biomass. The efficiency of the gasifier was predicted by changing the mixing ratio of coal with biomass, feed flow rate, and oxygen-to-carbon ratio. Three biomasses were used including rice husk, sugarcane bagasse, cotton stalks, and lignite coal mixture. According to the results, mixing coal with biomass significantly impacted the syngas composition, char conversion, and operational temperature. The mole fraction of CO was achieved at 0.344, and the H_2 mole fraction was obtained at 0.155 with 10% coal and 90% rice husk at 0.1 kg/sec feed flow rate and 1.0 O/C ratio. Char conversion and syngas composition were significantly affected by varying O/C ratios. With an increasing O/C ratio from 0.8 to 1.2, the mole fraction of H_2 and CO in syngas composition increases and decreases. The optimum O/C ratio was found at 1.0. At this O/C ratio, the syngas exit temperature was observed at a minimum, and char conversion was observed at a maximum.*

***Keywords:** Mathematical Modelling, Partial Differential Equations, Navier Stoke's Equation, Energy Equation, Computational Fluid Dynamics*

1. INTRODUCTION

Several mathematical sub-models are required to model coal gasification to describe the complex turbulent multiphase reacting flow system [1-3]. The relevance and applicability of the final simulation result are directly dependent on the quality and applicability of these sub-models, and efficient feedstock conversion is especially important in coal gasification. In recent decades, with rapid industrialization, urbanization, and economic and population growth energy usage on a global scale has risen dramatically [4, 5]. Fossil fuels have been a basic energy source for humanity [6-8]. Middle East, Asia, Africa, and other developing countries use oil, coal, and natural gas as their primary energy source [9]. For transportation, natural gas and oil have been used as primary fuel sources, while for electricity generation, coal is used. On the other hand, fossil fuel's natural reserves are depleting fast [10]. Oil and gas supplies may not last more than 50–60 years at present utilization rates, however, coal resources may last up to 200 years [11]. Furthermore, fossil fuels are one of the major sources of greenhouse gas emissions these emissions are liable for climate change and global warming [12]. When fossil fuels are burnt in engines and powerplants, they produce harmful emissions like carbon dioxide (CO_2), compounds of nitrogen oxides (NOx), and compounds of Sulphur dioxides (SOx) [13]. From 1970 to 2015, the global CO_2 emission was raised by 16 Gton to 36.25 Gton and it is estimated that out of 36.25 Gton, 11Gton was only produced by coal-based power plants and other sources of heat generation [14]. Global concerns about energy security and the threat of climate change have sparked intensive studies into carbon-neutral alternative and renewable energy sources [15, 16]. Although there are multiple sources of electricity generation, the lowest capital and operating cost is offered by the coal-thermal route thus they provide the smallest per unit cost [17, 18]. There are different ways coal is used as an energy source i.e., gasification pyrolysis and combustion [19]. The combustion pathway entails producing steam from the energy generated during coal combustion and using that steam to power the turbines. In contrast, the gasification pathway implies partial oxidation of coal to produce a mixture of gases like CO, H_2, CO_2, and other hydrocarbons in small proportion. Then it is used as fuel to fire the engine coupled with a generator set.

The main operational issue in coal gasification is incomplete char conversion owing to delayed oxidation kinetics. This incomplete char oxidation reduces the energy efficiency of coal gasification and becomes the reason for particulate emissions. Generally, for fluidized bed gasifier fuel having high char reactivity is preferred. Fuels with a high char reactivity are favored for a fluidized bed gasifier [20-22] and raising the operating temperature to improve conversion efficiency [23]. Hence, biomass and coals with low rank (lignite) are the most proper feedstocks. Higher rank coals are usually processed if the gasification process includes a residual char combustion stage [24, 25], if the gasifier is run under ash agglomerating conditions [26, 27]. Other possible benefits of this method include that the fuel does not need to be ground as finely as it does for entrained flow gasification, which is beneficial for fuels like biomass. Furthermore, the operating temperature is below the ash softening point, eliminating the risk of corrosive/melting ash. In a gasifier, the oxy-fuel gasification uses O_2 mixed with CO_2 and possibly steam as a substitute for conventional gases. The exhaust gas from this design is a CO_2/steam combination when combusted in a turbine. A part of this is reprocessed to support the inlet process stream with added O_2 and the remaining is open for sequestration. Any further development of the concept, on the other hand, would ideally need to be fuel adaptable, able to run on a variety of coals as well as, ideally, biomass. Biomass gasification is considered CO_2 neutral reducing fossil fuel dependence and sequestration of CO2 has resulted in a negative C footprint for the power plant. Waste biomass gasification also prevents the need to landfill / composite material, which results in undesirable emissions. Co-processing coal and biomass has potential benefits, Spiegl et al [28] found that co-gasification of Polish coal with silver birch wood in a pressurized fluidized bed reactor (4 barg, 700–900^{o}C) resulted in greater carbon conversion than gasification of the coal alone. Co-gasification of coal with olive bagasse (a waste material from the olive oil industry) was claimed to be effective by Andre et al [29]. An atmospheric pressure fluidized bed reactor with a 70 mm internal diameter was employed in that investigation. A varied combination of air and steam was used to fluidize the bed. According to the findings, up to 40% of biomass by weight might be gasified with coal. Although gasification has many advantages, the main drawback is the production of excessive tar [30-32], seasonal dependency, broad size distribution, and variable proportion of solid fuel [33]. Even though coal is a fossil fuel, co-gasification with biomass can lessen its environmental effect while also addressing the issue of seasonal reliance [34-36]. According to research, biomass improves the overall reactivity of coal by containing relatively high volatiles, which boosts the rate of heterogeneous reactions [37, 38]. As the complexity of these modeling and simulation operations has grown, greater depth in the underlying sub-models and processes has been necessary to produce accurate and meaningful results. Furthermore, as high-performance computer resources become more widely available, simulation tools are increasingly being employed to better understand and optimize the complicated reactive multiphase flow in coal gasification systems [39]. CFD simulations are becoming increasingly significant in the design of modern reactors.

This study investigated biomass and lignite coal dynamics using an entrained-flow MOB gasifier. As scant literature is available on the gasification of biomass and coal through the application of CFD using an entrained-flow MOB gasifier.

1.1 Fundamentals of Gasification

The carbon conversion efficiency using gasification is higher as compared with combustion, and in gasification, less quantity of oxygen is required. Carbon monoxide, hydrogen, and methane are the main products of the gasification process. The main chemical reaction involved during gasification is given as under.

Combustion-Reactions

$$C + \frac{1}{2}O_2 \rightarrow CO \quad \left(-111\frac{MJ}{kmol}\right) \quad (1)$$

$$CO + \frac{1}{2}O_2 \rightarrow CO_2 \quad \left(-283\frac{MJ}{kmol}\right) \quad (2)$$

$$H_2 + \frac{1}{2}O_2 \rightarrow H_2O \quad \left(-242\frac{MJ}{kmol}\right) \quad (3)$$

- Other Gasification Reactions

$$C + H_2O \leftrightarrow CO + H_2 \quad \left(131\frac{MJ}{kmol}\right) \quad (4)$$

$$C + CO_2 \leftrightarrow 2CO \quad \left(172\frac{MJ}{kmol}\right) \quad (5)$$

$$C + 2H_2 \leftrightarrow CH_4 \quad \left(-75\frac{MJ}{kmol}\right) \quad (6)$$

$$CO + H_2O \leftrightarrow CO_2 + H_2 \quad \left(-41\frac{MJ}{kmol}\right) \quad (7)$$

$$CH_4 + H_2O \leftrightarrow CO_2 + 3H_2 \quad \left(206\frac{MJ}{kmol}\right) \quad (8)$$

2. MATERIALS AND METHODS

2.1 Creating CAD Model and Computational Domain

The geometry of the multi-opposite burner was built with Ansys Design Modeler® 14.0, whereas Ansys Mesh®14.0 was used for mesh development. Ansys Fluent®14 was used for CFD Computations and solution of governing equations. The post-processing of results was done through the Ansys CFD Post®14 version. The diameter of the MOB was set at 1m, and the height of the MOB was taken as 4.2 m for feedstock gasification. Figure 1 shows the methodology of CFD simulation, coal, biomass sample preparation, and characterization. Fig. 2(a-b) shows the 3D top and front views of geometry, whereas Fig. 2(c) shows the 2D symmetric meshed domain of the geometry. With a minimum orthogonal quality of 0.689, the meshed geometry had 58,382 quadrilateral cells.

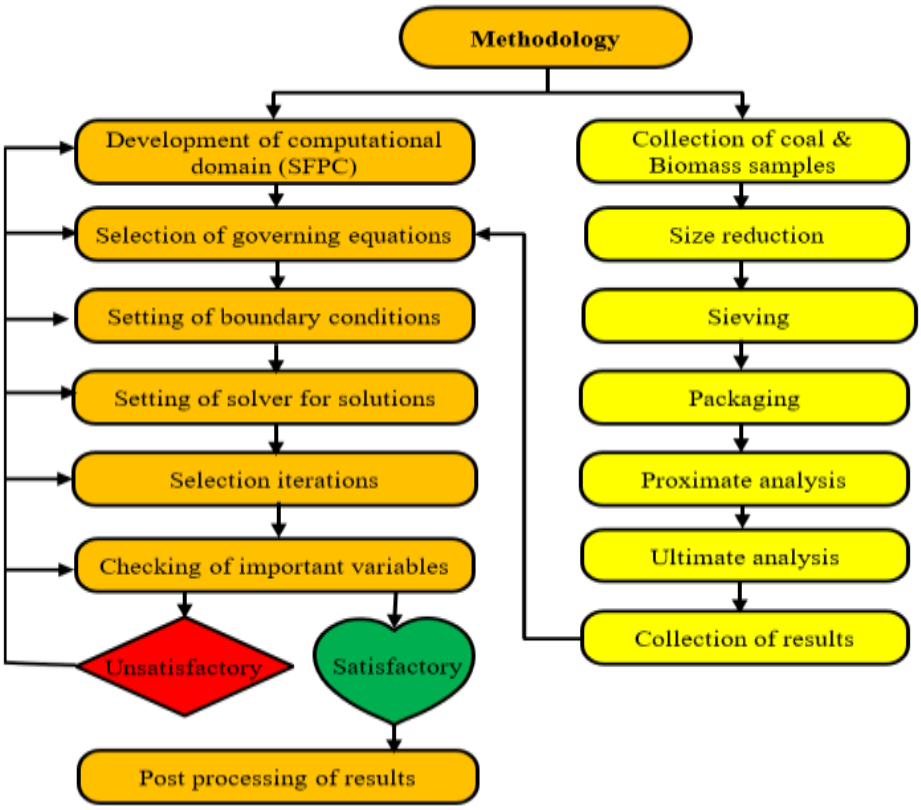

Fig. 1. Methodology for CFD simulation, coal, biomass sample preparation and characterization.

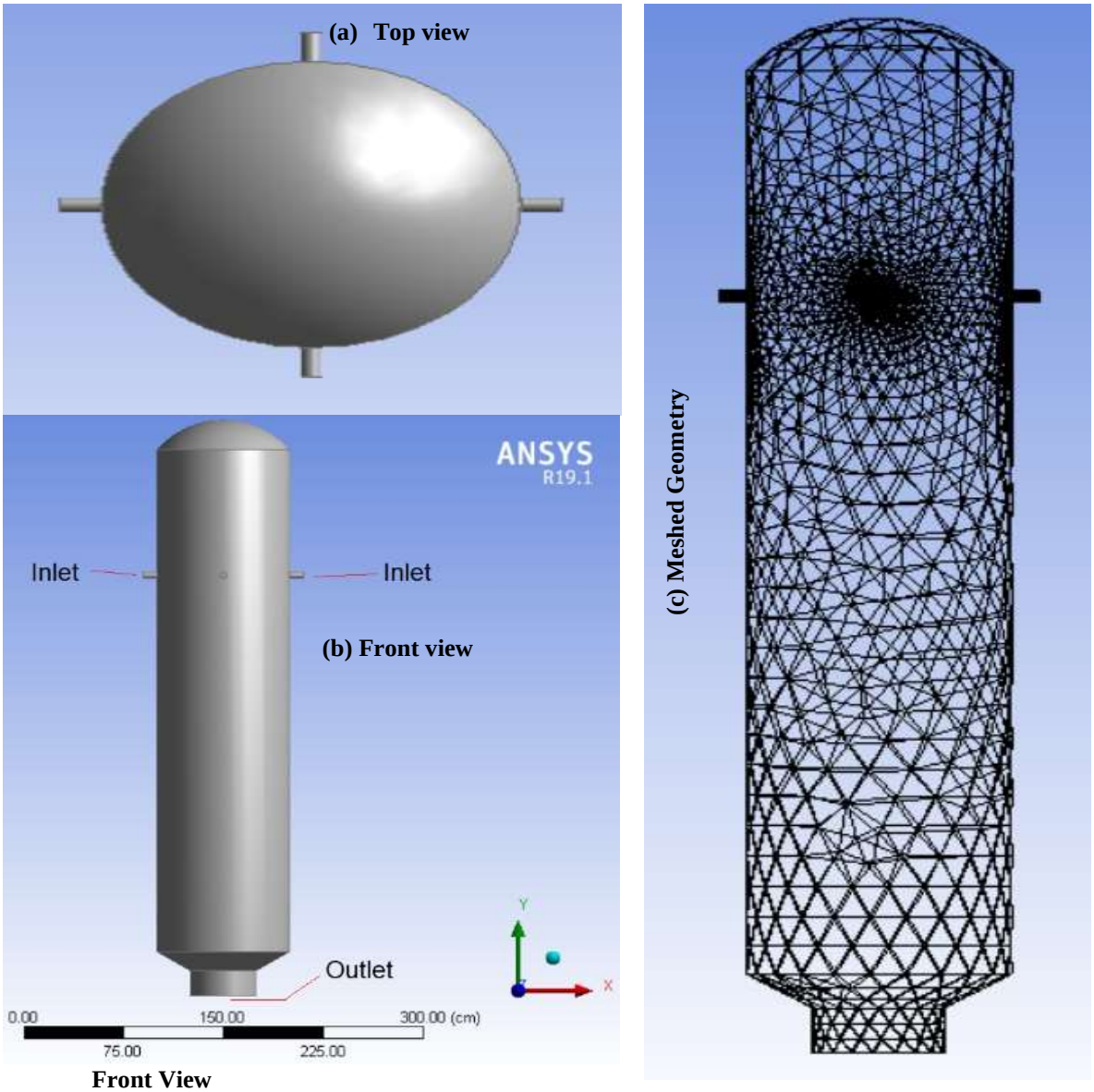

Fig. 2 (a-c) Top view, front view of 3D and meshed geometry of MOB gasifier**.**

2.2 GOVERNING EQUATIONS

The governing equations in this simulation study include momentum, mass, energy, and steady-state Navier Stokes equations. Furthermore, the heterogeneous and homogenous reactions were modeled [40].

$$\frac{\partial}{\partial x_i}\left(\rho u_{ij}\right) = S_m \tag{9}$$

$$\frac{\partial}{\partial x_i}\left(\rho u_i u_j\right) = \rho \bar{g}_j - \frac{\partial P}{\partial x_i} + \frac{\partial}{\partial x_i}\left(\tau_{ij} - \rho\overline{u'_i u'_j}\right) + S_j \tag{10}$$

$$\frac{\partial}{\partial x_i}\left(\rho c_p u_i T\right) = \frac{\partial}{\partial x_i}\left(\lambda \frac{\partial T}{\partial x_i} - \rho c_p \overline{u'_i T'}\right) + \mu\Phi + S_h \tag{11}$$

$$\frac{\partial}{\partial x_i}(\rho u_i C_j) = \frac{\partial}{\partial x_i}\left(\rho D_i \frac{\partial C_j}{\partial x_i} - \rho\overline{u'_i C'_j}\right) + S_r \qquad (12)$$

Here τ_{ij} represents symmetric stress and $\rho\overline{u_i' u_j'}$ is represents Reynold's stress. Whereas *k –ε was* applied to explain the flow of turbulence and turbulence kinematic viscosity was assessed using Eq. (13).

$$\mu_{t=\rho C_\mu k^2/\varepsilon} \qquad (13)$$

$$\frac{\partial}{\partial x_i}(\rho u_i k) = \frac{\partial}{\partial x_i}\left[\left(\mu + \frac{\mu_t}{\sigma_k}\right)\frac{\partial k}{\partial x_i}\right] + G_k - \rho\varepsilon \qquad (14)$$

$$\frac{\partial}{\partial x_i}(\rho u_i \varepsilon) = \frac{\partial}{\partial x_i}\left[\left(\mu + \frac{\mu_t}{\sigma_\varepsilon}\right)\frac{\partial \varepsilon}{\partial x_i}\right] + C_{1\varepsilon}G_k\frac{\varepsilon}{k} - C_{2\varepsilon}G_k\frac{\varepsilon^2}{k} \qquad (15)$$

The kinetic energy generation due to the gradient of mean velocity is G_k. Heat conductivity of turbulence is represented by (λ), and coefficient diffusion is (D) in Eqs. 11 and 12.

$$\rho c_p \overline{u'_i T'} = -\lambda\frac{\partial T}{\partial x_i} = c_p\frac{\mu_t}{Pr_t}\frac{\partial T}{\partial x_i} \qquad (16)$$

$$\rho\overline{u'_i C'_j} = -\rho D_i\frac{\partial C_j}{\partial x_i} = \frac{\mu_t}{Sc_t}\frac{\partial C_j}{\partial x_i} \qquad (17)$$

The value of the Prandtl number for turbulence is 0.85, whereas the Schmidt number is 0.7 for turbulence.

2.3 Discrete Phase Modeling

Euler Lagrangian approach was used through a discrete phase model to investigate the particle motion trajectories during continuous movement of fluid phases and can be written as.

$$\frac{du_p}{dt} = F_d(u - u_p) + g_x\frac{\rho_p - \rho}{\rho_p} + F_x \qquad (18)$$

$$-\nabla q_r = aG - 4aG\sigma T^4 \qquad (19)$$

$$q_{r=-\frac{1}{3(a+\sigma_s)-C\sigma_s}}\nabla G \qquad (20)$$

2.4 Combustion / Gasification Model

The decomposition of biomass and coal occurs mainly in volatile species, char and ash, at high temperatures and can be represented as.[41, 42].

$$Coal/Biomass \rightarrow \alpha_1 volatiles + \alpha_2 H_2O + \alpha_3 Char + \alpha_4 Ash \qquad (21)$$

$$Coal/Biomass \xrightarrow{k_l} (1 - Y_l) \times Char_l + Y_l \times Volatile \quad for\ low\ temperature \qquad (22)$$

$$Coal/Biomass \xrightarrow{k_h} (1 - Y_h) \times Char_h + Y_h \times Volatile \quad for\ high\ temperature \qquad (23)$$

$$\frac{dV}{dt} = (K_l Y_1 + K_h Y_h) Coal \qquad (24)$$

$$K_l = A_l \, esp\left(E_l / RT_p\right) \qquad (25)$$

$$K_h = A_h \, esp\left(E_h / RT_p\right) \qquad (26)$$

In gasification of coal mainly generates char, hydrogen, and carbon monoxide. Various researchers have explained the mechanism of gasification reactions [40, 43-51]. The Eddy dissipation rate model calculated each species formation rate of each species.

$$S_r = M_j \sum_{j=1}^{N} w_{j,r} \qquad (27)$$

$$w_{j,r=(v''_{j,r} - v'_{j,r})} k_f \left(\prod_{i=1}^{Nr} [C]^{n''} - \frac{1}{K_{eq}} \prod_{i=1}^{Nr} [C]^{n''} \right) \qquad (28)$$

$$k_f = AT^B e^{\left(-E_a / RT\right)} \qquad (29)$$

The rate constant for a forward reaction was obtained by Arrhenius law, and *Kf* represents the rate constant. While *A* represents the pre-exponential factor and *Ea* shows activation energy.

2.5 NOx and SOx modeling

Modeling and simulation for NOx and SOx prediction were done through the application of ANSYS Fluent. During the simulation of prompt NOx and SOx, subsequent mass transfer equations were solved.

$$\frac{d}{dt}(\rho Y_{NO}) = \nabla.(\rho D \nabla Y_{NO}) + S_{NO} \qquad (30)$$

$$\frac{\partial}{\partial t}(\rho Y_{HCN}) + \nabla.(\rho \vec{v} Y_{HCN}) = \nabla.(\rho D \nabla Y_{HCN}) + S_{HCN} \qquad (31)$$

$$\frac{\partial}{\partial t}\left(\rho Y_{NH_3}\right) + \nabla.\left(\rho \vec{v} Y_{NH_3}\right) = \nabla.\left(\rho D \nabla Y_{NH_3}\right) + S_{NH_3} \qquad (32)$$

$$\frac{\partial}{\partial t}\left(\rho Y_{N_2O}\right) + \nabla \cdot \left(\rho \vec{v} Y_{N_2O}\right) = \nabla \cdot \left(\rho D \nabla Y_{N_2O}\right) + S_{N_2O} \qquad (33)$$

$$\frac{\partial}{\partial t}\left(\rho Y_{SO_2}\right) + \nabla \cdot \left(\rho \vec{v} Y_{SO_2}\right) = \nabla \cdot \left(\rho D \nabla Y_{SO_2}\right) + S_{SO_2} \qquad (34)$$

$$\frac{\partial}{\partial t}\left(\rho Y_{H_2S}\right) + \nabla \cdot \left(\rho \vec{v} Y_{H_2S}\right) = \nabla \cdot \left(\rho D \nabla Y_{H_2S}\right) + S_{H_2S} \qquad (35)$$

$$\frac{\partial}{\partial t}\left(\rho Y_{SO_3}\right) + \nabla \cdot \left(\rho \vec{v} Y_{SO_3}\right) = \nabla \cdot \left(\rho D \nabla Y_{SO_3}\right) + S_{SO_3} \qquad (36)$$

$$\frac{\partial}{\partial t}(\rho Y_{SO}) + \nabla \cdot (\rho \vec{v} Y_{SO}) = \nabla \cdot (\rho D \nabla Y_{SO}) + S_{SO} \qquad (37)$$

2.6 Boundary conditions and calculation methods

The development of a 3D computational domain having quadrilateral cells 58382 was established using ANSYS Fluent. The inlet boundary conditions were set as mass flow and pressure flow at outlet boundary conditions. The temperature of the walls was kept constant at 800K and was maintained through a cooling water system. The inlet boundary condition was represented by mass flow and outlet boundary conditions were represented as pressure

outlet. The solution converged when mass transfer, turbulent kinetic energy, and momentum residuals were satisfied at 10^{-3} and residuals for energy and radiation at 10^{-6}.

Table 1. Proximate and ultimate analysis of biomass and Thar Coal [52]

Biomass type	**SB**	**RH**	**CS**	**Proximate Analysis of Thar Coal**	
Proximate Analysis (wt. % dry basis)				Element	Value (wt.%)
M	5.8	6.10	5.58	M	44.3
VM	74.87	63.39	69.98	VM	29.55
FC	14.93	15.96	16.31	FC	19.21
Ash	4.40	14.55	8.13	Ash	6.83
Ultimate investigation results on (wt. % dry basis)				Ultimate investigation results on (wt.% MF)	
O	49.39	50.43	52.05	C	38.17
H	5.96	5.36	5.82	H	7.93
S	0.19	0.59	0.30	N	0.23
C	44.1	43.33	41.73	O	6.84
N	0.36	0.29	0.10	S	1.87
HHV (MJ/Kg)	17.33	13.86	16.22		

3. RESULTS AND DISCUSSIONS

3.1 Biomass to Coal Mixing Ratio Effect

Rice husk, cotton stalks, and sugarcane bagasse were gasified separately by different mixing ratios. The biomass and coal feeding flow rates were fixed at 0.1 kg/sec and the oxygen/carbon ratio was maintained at 1.0 respectively. The effect was measured keeping in view three operating parameters: effect on syngas composition, char conversion, and temperature.

3.2 Syngas Composition at a Varying Mixing Ratio

Fig. 3(a) shows the effect of different mixing ratios of thar coal with cotton stalks and their impact on syngas composition. The composition of syngas is significantly affected by varying mixing ratios. In the syngas composition, the mole fractions of carbon monoxide and hydrogen at 100 percent cotton stalks were observed at 0.2720 and 0.197 respectively. Furthermore, at a mixing ratio of 70 cotton stalks and 30% coal maximum mole fractions of CO were observed at 0.287, while the mole fractions of H_2 decreased slightly to 0.162. Moreover, Fig. 3 (b-c) shows the effect of the mixing ratio on syngas composition using sugarcane bagasse and rice husk as feedstocks. In syngas composition, the maximum mole fractions of CO and H2 were achieved at a mixing ratio of 80% rice husk and 20% coal of 0.332 and 0.145 respectively. Whereas for sugarcane bagasse, the maximum mole fractions of CO and H_2 in syngas composition were observed at 0.287 and 0.1885 using a sugarcane bagasse of 90% and a coal mixing ratio of 10%.

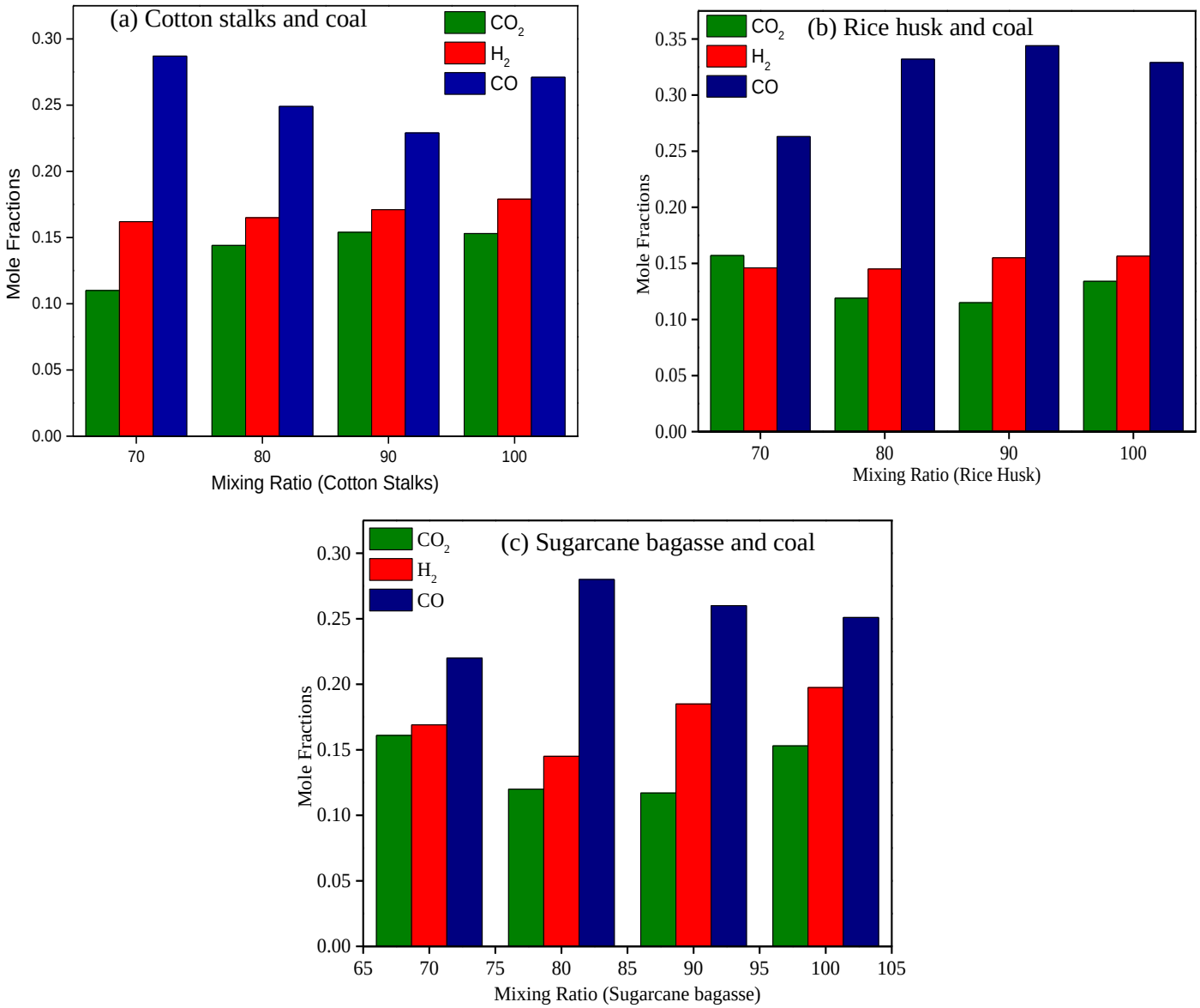

Fig. 3 (a-c) Shows the Mole fractions of CO, CO_2, and H_2 produced in syngas composition using varying mixing ratios of selected biomasses with thar coal.

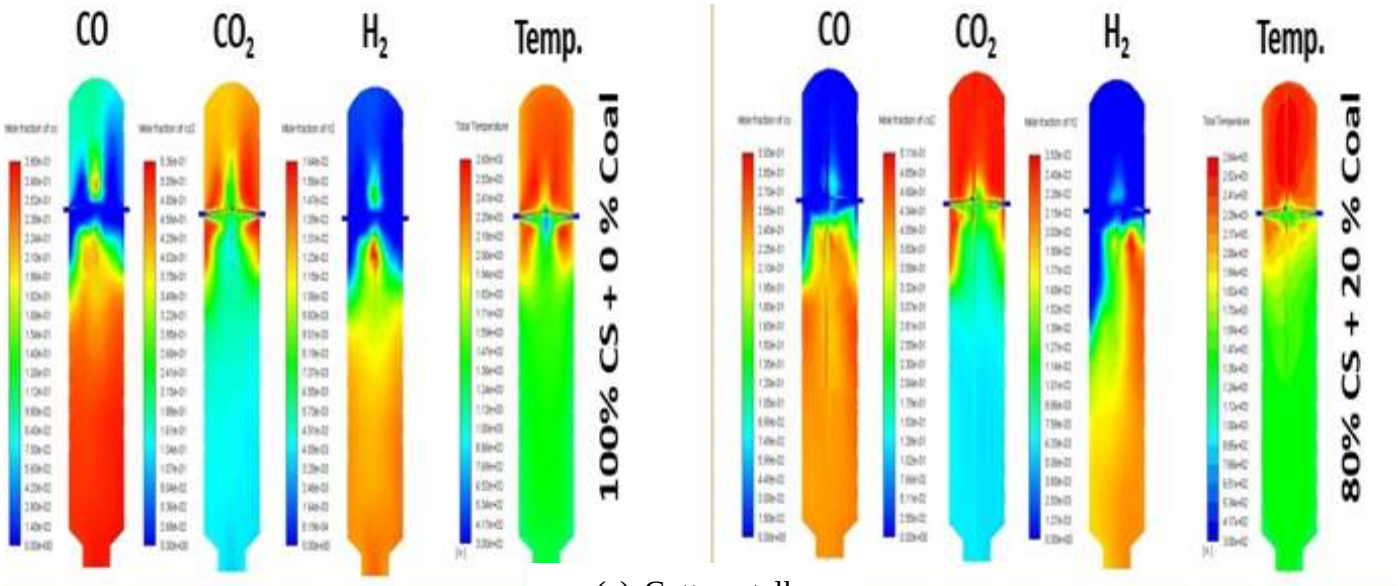

(a) Cotton stalks

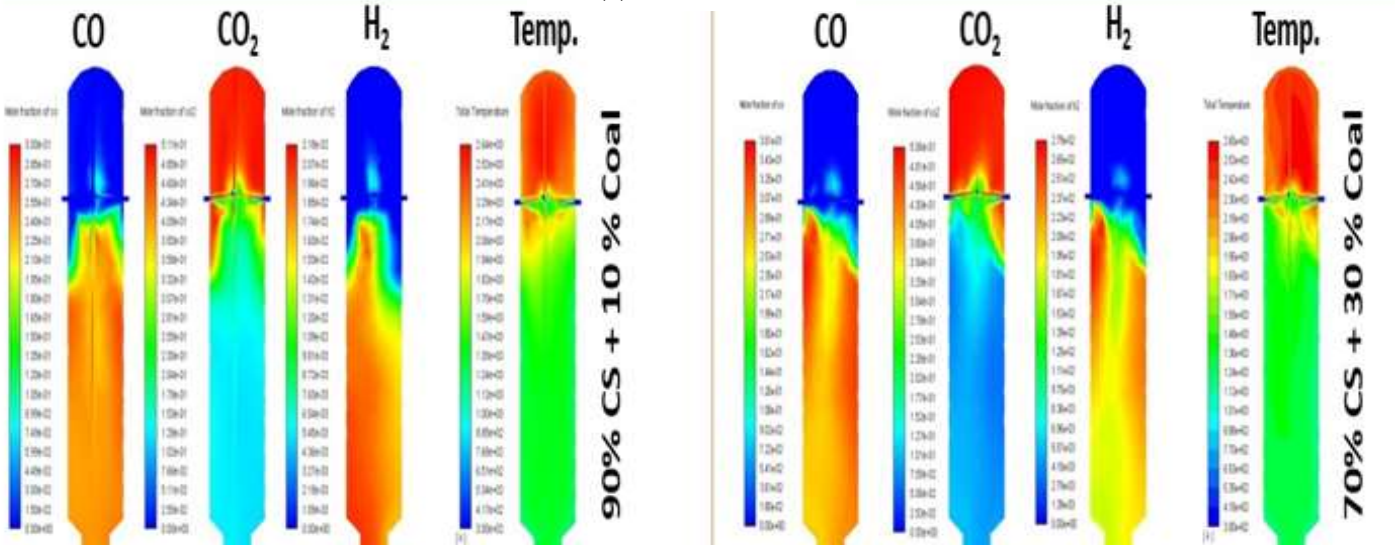

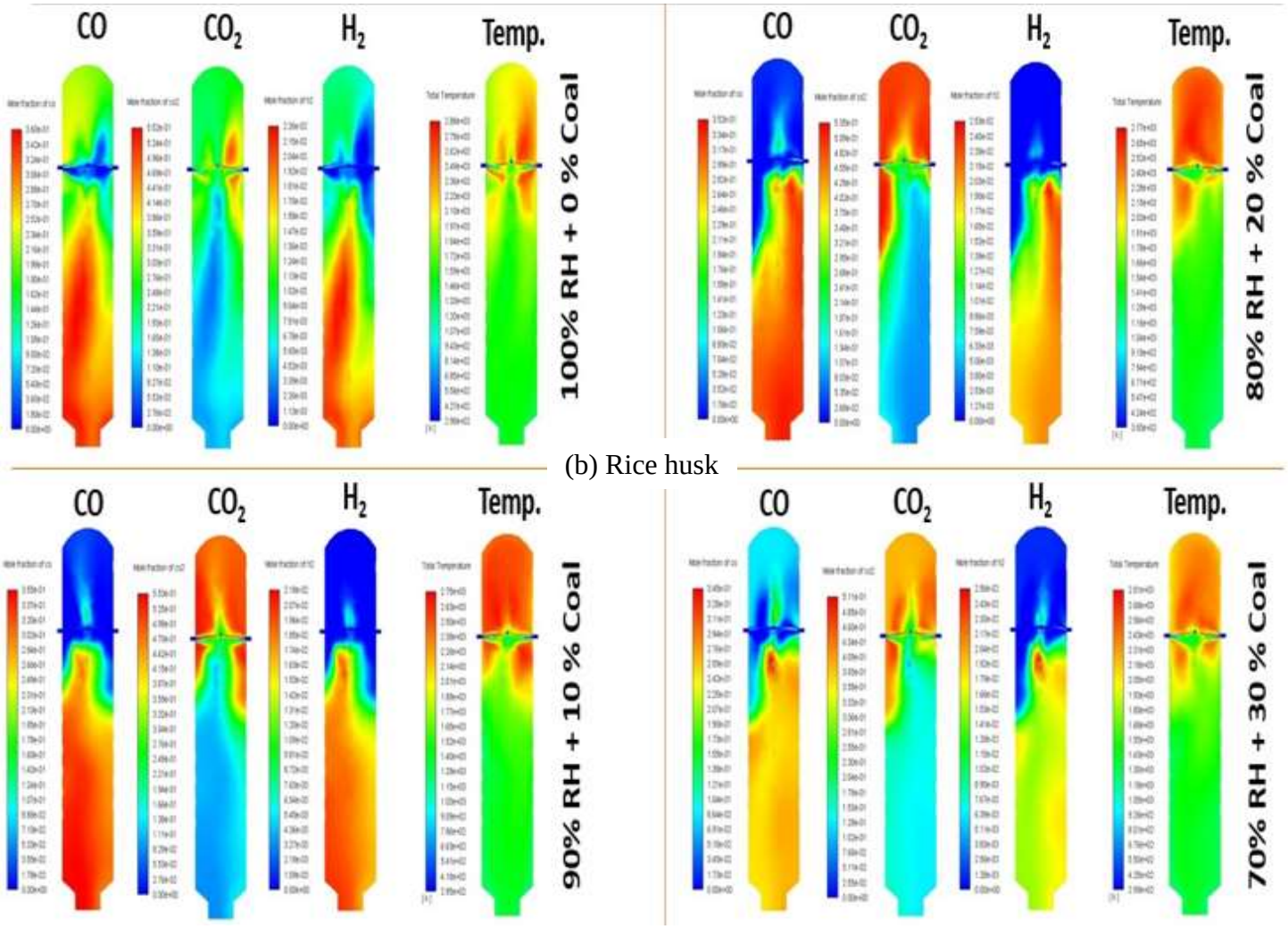
CO
CO_2
H_2
Temp.
100% RH + 0 % Coal
80% RH + 20 % Coal
90% RH + 10 % Coal
70% RH + 30 % Coal

(b) Rice husk

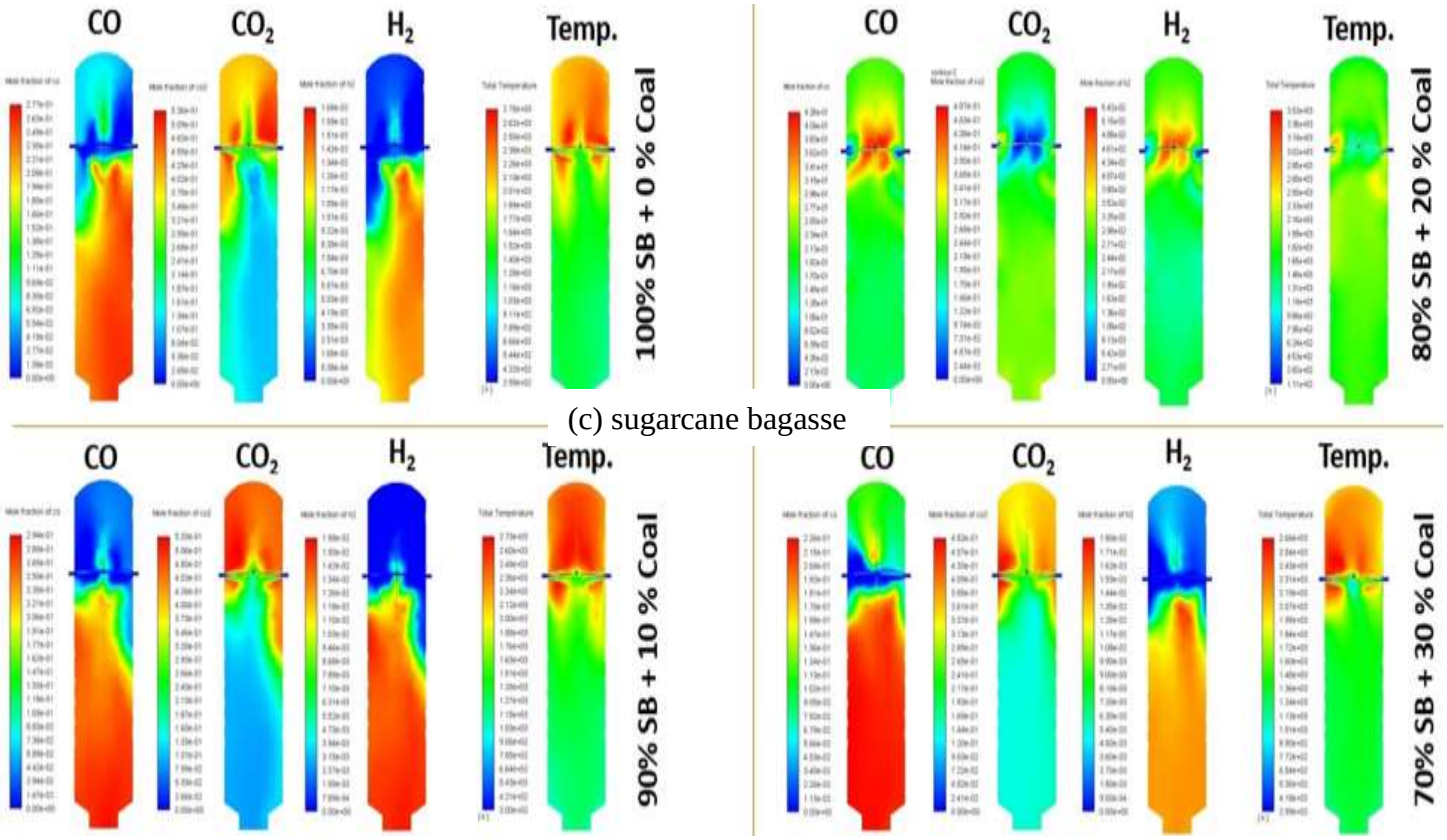

Fig. 4 (a-c) Contours showing mole fractions of CO, CO_2, H_2 species and temperature contours using (a) cotton stalks, (b) rice husk (c) sugarcane bagasse at different mixing ratios with Thar Coal at O/C ratio 1.0 and Feeding flow rate of 0.1kg/sec.

3.3 Syngas Exit Temperature and Char Conversion at a Varying Mixing Ratio

Figure 5(a-c) shows the char conversion and syngas temperature for all three selected biomasses. The char conversion at a mixing ratio of 80% cotton stalks and 20% coal was achieved the maximum of 96.88%, whereas, in the case of 90% rice husk and 10% coal, the highest char degradation was attained at 99.92%. Furthermore, having a mixing ratio of 80% sugarcane and 20% coal the highest char conversion was obtained at 98.5%. Whereas at a feeding rate of 0.1 kg/sec and a 1.0 O/C ratio for 80% sugarcane bagasse and 20% coal, the syngas maximum outlet temperature was noted 1969 K.

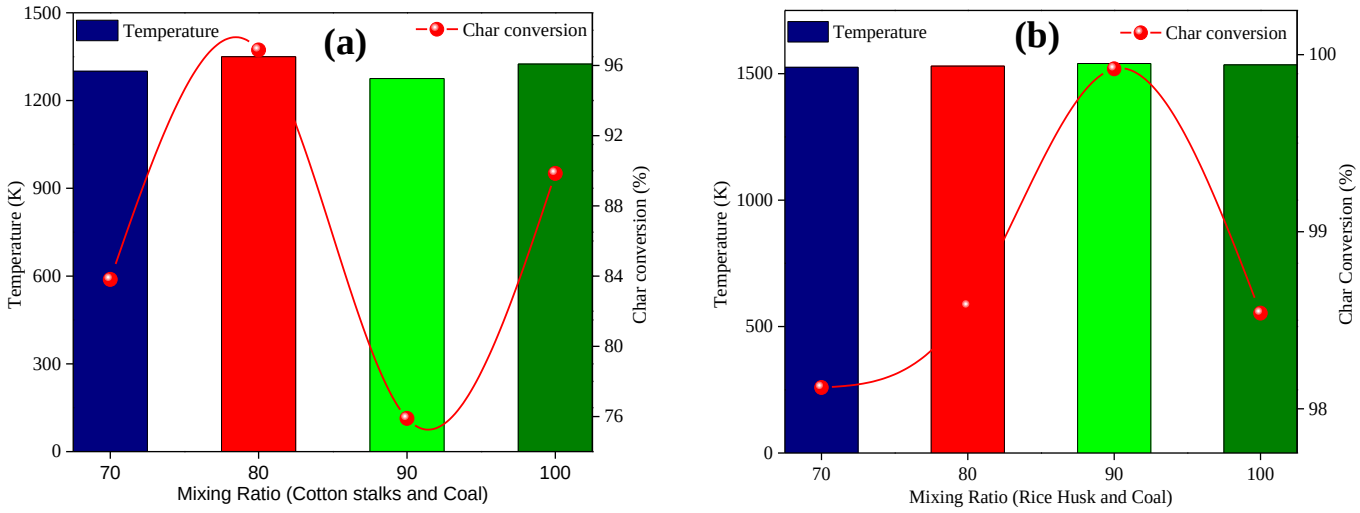

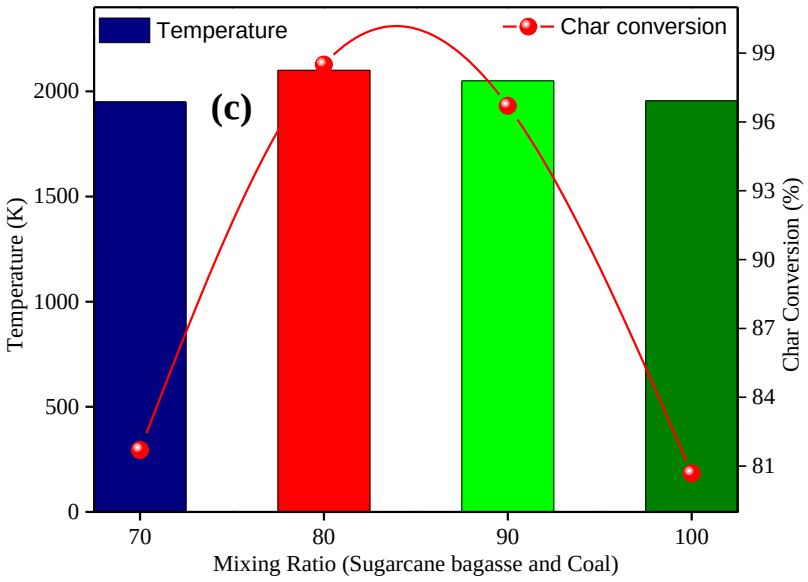

Fig. 5 (a-c) shows char conversion and syngas exit temperature at a different mixing ratio of selected biomasses and coal.

3.4 Effect of O/C Ratio on Syngas Composition

The effect of variations in O/C ratio on mole fractions of CO, CO_2 and H_2 in the synthesis using 90% rice husk and 10% coal is shown. At an O/C ratio of 0.8, the mole fractions of CO were observed 0.281 and further increased up to 0.344 at an O/C ratio of 1.0. When the O/C ratio was further increased to 1.2, mole fractions of CO in syngas composition decreased to 0.274. the decrease in CO production at a higher O/C ratio was due to the dominance of combustion reactions producing more CO_2 than gasification reactions. Furthermore, the H_2 production was observed at 0.142 at 0.8 O/C, whereas H_2 mole fractions were further increased to 0.155 at the O/C ratio of 1.0 and a further increase in O/C ratio reduced mole fractions of H_2 in syngas composition. The maximum CO_2 mole fractions were observed at 0.182 at 0.8 C/O ratios, whereas the minimum CO2 mole fractions achieved 0.115 at 1.0 O/C ratios. Therefore, the optimum O/C ratio for 90% rice husk and 10% lignite coal was observed at a 1.0 O/C ratio for getting mole fractions of CO and H_2 in syngas composition.

3.5 Effect of O/C Ratio on Char Conversion and Syngas Temperature

The effect of variations in O/C on syngas temperature and char conversion is shown in Fig. 7. The maximum conversion of char 98.73 was achieved at an O/C ratio of 1.0 and a minimum temperature of 1402K. Moreover, the minimum temperature suggests that gasification reactions are endothermic hence the temperature of syngas was reduced.

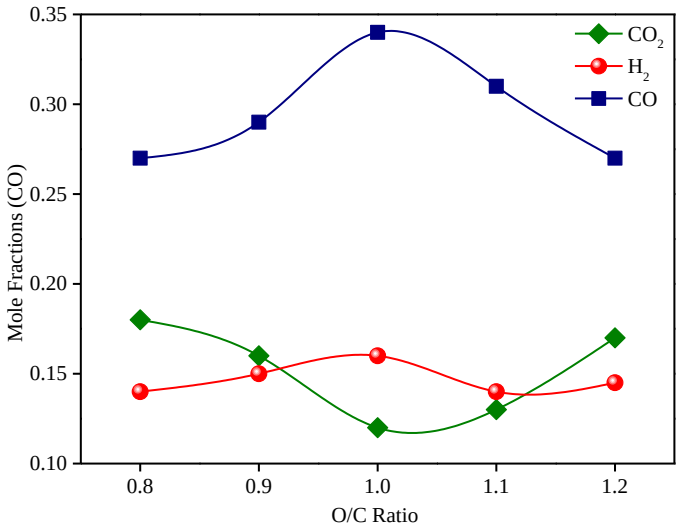

Fig. 6 Shows the effect of O/C variation on the composition of syngas utilizing 90% rice husk and 10% thar coal.

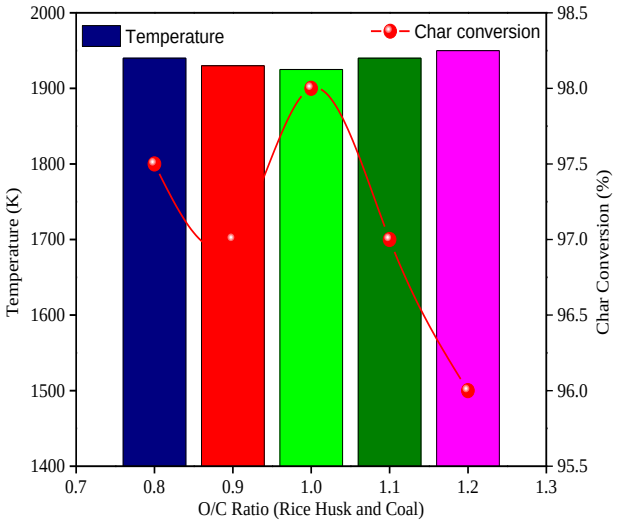

Fig.7 Shows exit syngas temperature along with char conversion utilizing 90% rice husk and 10% Thar Coal as feedstock at varying O/C ratios.

3.6 Effect of Feeding Rate On Syngas Composition

Figure 8 shows mole fractions of syngas components at different feeding flow rates. The feed flow of biomass and coal ranged from 0.1 kg/sec up to 0.5 kg/sec, whereas the O/C ratio was maintained at 1.0 for 90% rice husk and 10% coal to get an optimized feed flow rate. The feeding rate on syngas composition such as CO, CO_2, and H_2, char conversion, and temperature were investigated. With the increase in feed flow rate, the mole fractions of vital elements in syngas composition CO and H_2 decreased. In contrast, the mole fractions of CO_2 in syngas composition increased with increasing feeding flow. Moreover, the MOB gasifier's optimized performance was achieved at a feed flow rate of 0.1kg/sec.

3.7 Effect of Feeding Rate on Char Conversion and Syngas Temperature

Figure 9 shows the trend of syngas temperature and char conversion at different feed flow rates. More specifically, the char conversion was decreased with an increase in feeding rate, besides that the temperature was also increased. Therefore Fig. 9 represents the effect of varying feed flow rates on char conversion and syngas temperature.

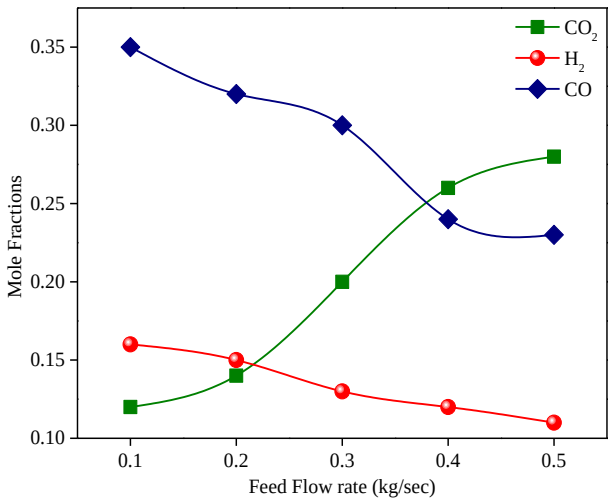

Fig. 8 Shows the behavior of syngas using 90% rice husk and 10% coal at varying feeding flow rates.

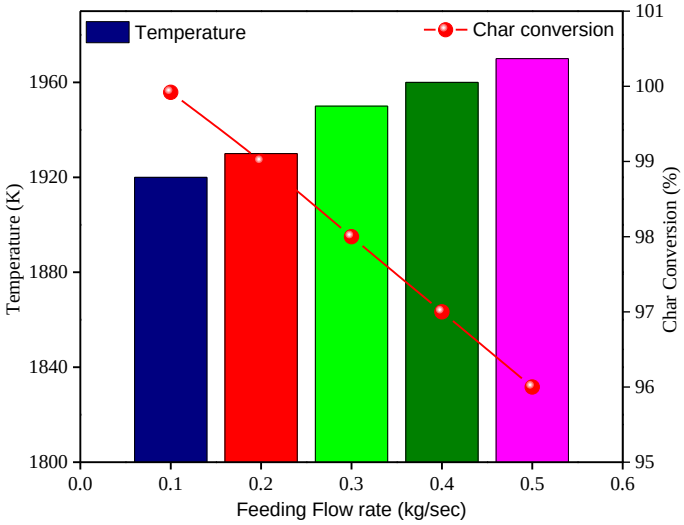

Fig. 9 Represents syngas temperature and char conversion trend at 90% rice husk and 10% thar coal using varying feeding rates.

3.8 Estimation of SOx and NOx

Rice husk and coal mixture at a fixed feeding rate of 0.1kg/sec was used to estimate NOx and SOx emissions. The NO_x emissions at varying O/C ratios of rice husk and coal are given in Fig. 10. The SOx emissions decreased with an increase in O/C ratio suggesting that combustion reactions dominate over gasification reactions producing fewer emissions of SOx. Gasification of biomass without mixing with coal generates higher emissions of SOx. Because of the high sulfur content in biomass, its gasification produces more SOx emissions compared to the different mixing ratios of coal and biomass feedstocks. The maximum concentration of SOx in syngas composition using 100% rice husk was observed at 4235 ppm at an O/C of 0.8, while the minimum concentration of SOx in syngas composition was found at 2457 ppm at a missing ratio of 70% rice husk and 30% coal at 1.2 O/C ratio respectively. Fig. 10 shows the SOx generation at varying rice husk and coal mixing rates and using different O/C ratios.

According to the National Environmental Quality Standards (NEQS) of Pakistan, the maximum limit of SOx (mostly in the form of SO_2) from any power plant should be less than 800 mg/Nm^3, equivalent to 14500 ppm. So, comparing the simulated SOx estimation with the standard, it has been found that the gasifier produces much less SOx than NEQS standards. The maximum concentration of NOx in syngas composition using 100% rice husk was achieved at 268.6 ppm at a 1.2 O/C ratio. The minimum concentration of NOx emissions was found using 70% rice husk and 30% coal at 168.5 ppm at 0.8 O/C ratios.

The generation of NOx emissions increased with an O/C ratio irrespective of the feedstock and its varying mixing ratios. The behavior of NOx emissions during gasification at varying mixing rates and O/C ratios is shown in Fig. 11. More specifically, the NOx emissions during alone gasification of rice husk are higher than the co-gasification of rice husk and coal at different mixing ratios due to higher concentration of nitrogen in rice husk composition and dominance of combustion reactions.

According to the National Environmental Quality Standards (NEQS) of Pakistan, the maximum limit of NOx (mostly in the form of NO_2) from any power plant operated on coal should be less than 240 ppm. The comparison of simulated results with standard gives an idea that a few simulated results are smaller than provided standard limit, however most of the case results are less than the NOx limits.

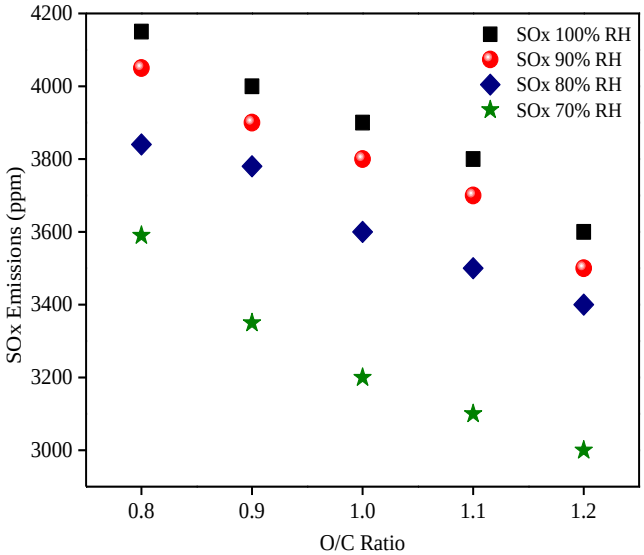

Fig. 10. Emissions of SOx using rice husk and coal feedstocks at varying O/C ratios.

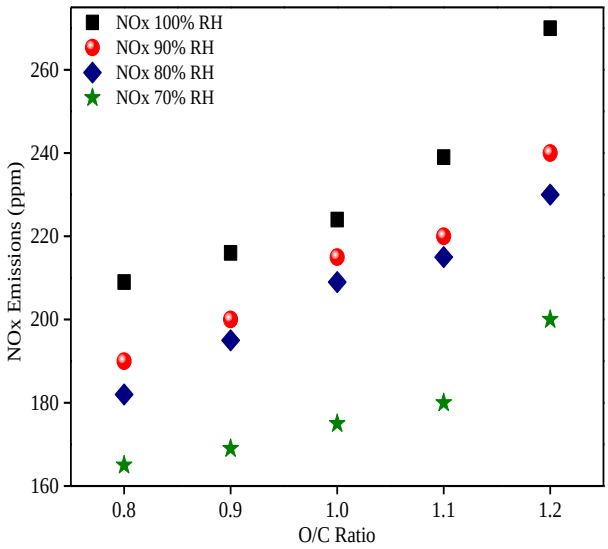

Fig. 11. Emissions of NOx using rice husk and coal feedstocks at varying O/C ratios.

4. CONCLUSIONS

The entrained flow gasifier with multi-opposite burners was numerically simulated in the present study to inspect the behavior of biomass gasification with a Thar lignite mixture. ANSYS FLUETNT®14 was used for modeling and simulation purposes. In simulations, the solid gas phase and their interactions were solved using the Euler-

Lagrangian framework. The effect of different biomass/coal mixing ratios, char conversion, temperature, and syngas compositions were investigated. Furthermore, the generation of SOx and NOx were also investigated through modeling and simulations. The finding of this study is summarized as follows.

- At a mixing ratio of 80% sugarcane bagasse and 20% coal maintaining an O/C ratio of 1.0 and a feeding flow rate of 0.1kg/sec, the maximum syngas temperature at the MOB exit was achieved at 1969 K.
- The variations in O/C ratio from 0.8 to 1.2 significantly affect char conversion and synthesis gas composition, the increase in H_2 and CO mole fractions was initially observed then the mole fraction decreased.
- At O/C ratio 1.0, the maximum char conversion and minimum syngas exit temperature were recorded.
- An increase in feed flow rate results in decreased mole fractions of CO and H_2, whereas the mole fractions of CO_2 were also increased with an increase in feed flow rate. The increase in feed flow rate reduced char conversion.
- The increase in coal mixing with biomass decreased the SOx and NOx emissions. Moreover, with an increase in the O/C ratio, NOx emissions increased, and SOx emissions reduced significantly.
- The maximum SOx emissions of 4235 ppm were noticed at a 0.8 O/C carbon ratio when 100% rice husk was gasified. At the same time, minimum SOx emissions were found at 2457 ppm by using 70% rice husk and 30% Thar coal at a 1.2 O/C ratio.
- At an O/C ratio of 1.2, the maximum NOx emissions were observed 268.6ppm from biomass, while the maximum NOx emissions of 168.5 ppm at 0.8 O/C ratios were observed using 70% rice husk and 30% Thar coal.

Acknowledgments

All authors acknowledge the research environment and facilities provided by IoBM, Mehran UET, and Dawood UET management throughout this research work.

References

1. Singh, R.I., A. Brink, and M. Hupa, CFD modeling to study fluidized bed combustion and gasification. Applied Thermal Engineering, 2013. 52(2): p. 585-614.
2. Kuang, S., Z. Li, and A. Yu, Review on modeling and simulation of blast furnace. steel research international, 2018. 89(1): p. 1700071.
3. Weber, R., et al., On predicting the ash behaviour using Computational Fluid Dynamics. Fuel Processing Technology, 2013. 105: p. 113-128.
4. Rehman, A., H. Ma, and I. Ozturk, Do industrialization, energy importations, and economic progress influence carbon emission in Pakistan. Environmental Science and Pollution Research, 2021. 28(33): p. 45840-45852.
5. Kongkuah, M., H. Yao, and V. Yilanci, The relationship between energy consumption, economic growth, and CO2 emissions in China: the role of urbanisation and international trade. Environment, Development and Sustainability, 2022. 24(4): p. 4684-4708.
6. Hazrati, M. and R. Heffron, Conceptualising restorative justice in the energy Transition: Changing the perspectives of fossil fuels. Energy research & social science, 2021. 78: p. 102115.
7. Londono-Pulgarin, D., et al., Fossil or bioenergy? Global fuel market trends. Renewable and Sustainable Energy Reviews, 2021. 143: p. 110905.
8. Fernández-Torres, M.J., W. Dednam, and J.A. Caballero, Economic and environmental assessment of directly converting CO2 into a gasoline fuel. Energy Conversion and Management, 2022. 252: p. 115115.
9. Ahmad, T. and D. Zhang, A critical review of comparative global historical energy consumption and future demand: The story told so far. Energy Reports, 2020. 6: p. 1973-1991.
10. Yaqoob, H., et al., Energy evaluation and environmental impact assessment of transportation fuels in Pakistan. Case Studies in Chemical and Environmental Engineering, 2021. 3: p. 100081.
11. Zou, C., et al., Energy revolution: From a fossil energy era to a new energy era. Natural Gas Industry B, 2016. 3(1): p. 1-11.
12. Al-Ghussain, L., Global warming: review on driving forces and mitigation. Environmental Progress & Sustainable Energy, 2019. 38(1): p. 13-21.
13. AYDIN, H. and C. İLKILIÇ, Air pollution, pollutant emissions and harmfull effects. Journal of Engineering and Technology, 2017. 1(1): p. 8-15.

14. Mallick, D., P. Mahanta, and V.S. Moholkar, Co-gasification of coal and biomass blends: Chemistry and engineering. Fuel, 2017. 204: p. 106-128.
15. Owusu, P.A. and S. Asumadu-Sarkodie, A review of renewable energy sources, sustainability issues and climate change mitigation. Cogent Engineering, 2016. 3(1): p. 1167990.
16. Yuan, X., et al., The race to zero emissions: Can renewable energy be the path to carbon neutrality? Journal of Environmental Management, 2022. 308: p. 114648.
17. Aneke, M. and M. Wang, Energy storage technologies and real life applications–A state of the art review. Applied Energy, 2016. 179: p. 350-377.
18. Akhtari, S., T. Sowlati, and K. Day, Economic feasibility of utilizing forest biomass in district energy systems–A review. Renewable and sustainable energy reviews, 2014. 33: p. 117-127.
19. Jayaraman, K. and I. Gökalp, Pyrolysis, combustion and gasification characteristics of miscanthus and sewage sludge. Energy Conversion and Management, 2015. 89: p. 83-91.
20. Hai, I.U., et al., Assessment of biomass energy potential for SRC willow woodchips in a pilot scale bubbling fluidized bed gasifier. Fuel, 2019. 258: p. 116143.
21. González-Vázquez, M.d.P., et al., Comparison of the gasification performance of multiple biomass types in a bubbling fluidized bed. Energy conversion and management, 2018. 176: p. 309-323.
22. Wan Ab Karim Ghani, W., et al., Air gasification of agricultural waste in a fluidized bed gasifier: hydrogen production performance. Energies, 2009. 2(2): p. 258-268.
23. Kulkarni, A., et al., Experimental study of torrefied pine as a gasification fuel using a bubbling fluidized bed gasifier. Renewable Energy, 2016. 93: p. 460-468.
24. Smoot, L.D. and P.J. Smith, Coal combustion and gasification. 2013: Springer Science & Business Media.
25. Unar, I.N., et al., Numerical study of coal composition effects on the performance of gasification through computational fluid dynamic. International Journal of Chemical Reactor Engineering, 2019. 17(7).
26. Salleh, M., et al., Gasification of biochar from empty fruit bunch in a fluidized bed reactor. Energies, 2010. 3(7): p. 1344-1352.
27. Usto, M.A., et al., Desulfurization of thar lignite by oxidative alkali leaching under pressure. International Journal of Coal Preparation and Utilization, 2021: p. 1-21.
28. Spiegl, N., et al., Oxy-fuel co-gasification of coal and biomass for negative CO2 emissions. Fuel, 2021. 306: p. 121671.
29. André, R.N., et al., Fluidised bed co-gasification of coal and olive oil industry wastes. Fuel, 2005. 84(12-13): p. 1635-1644.
30. Li, J., et al., Review of microwave-based treatments of biomass gasification tar. Renewable and Sustainable Energy Reviews, 2021. 150: p. 111510.
31. Rios, M.L.V., et al., Reduction of tar generated during biomass gasification: A review. Biomass and bioenergy, 2018. 108: p. 345-370.
32. Ren, J., et al., Recent advances in syngas production from biomass catalytic gasification: A critical review on reactors, catalysts, catalytic mechanisms and mathematical models. Renewable and Sustainable Energy Reviews, 2019. 116: p. 109426.
33. Asadullah, M., Barriers of commercial power generation using biomass gasification gas: A review. Renewable and Sustainable Energy Reviews, 2014. 29: p. 201-215.
34. Koukouzas, N., et al., Co-gasification of solid waste and lignite–A case study for Western Macedonia. Waste Management, 2008. 28(7): p. 1263-1275.
35. Lu, X., et al., Gasification of coal and biomass as a net carbon-negative power source for environment-friendly electricity generation in China. Proceedings of the National Academy of Sciences, 2019. 116(17): p. 8206-8213.
36. Mariyam, S., et al., A critical review on co-gasification and co-pyrolysis for gas production. Renewable and Sustainable Energy Reviews, 2022. 161: p. 112349.
37. Wang, G., et al., Thermal behavior and kinetic analysis of co-combustion of waste biomass/low rank coal blends. Energy Conversion and Management, 2016. 124: p. 414-426.
38. Ismail, T.M., et al., Coal and biomass co-pyrolysis in a fluidized-bed reactor: Numerical assessment of fuel type and blending conditions. Fuel, 2020. 275: p. 118004.
39. Wang, H., et al., A review of deep learning for renewable energy forecasting. Energy Conversion and Management, 2019. 198: p. 111799.
40. Silaen, A. and T. Wang, Effect of turbulence and devolatilization models on coal gasification simulation in an entrained-flow gasifier. International Journal of Heat and Mass Transfer, 2010. 53(9): p. 2074-2091.

41. Chen, W.-H., S.-W. Du, and T.-H. Yang, Volatile release and particle formation characteristics of injected pulverized coal in blast furnaces. Energy Conversion and Management, 2007. 48(7): p. 2025-2033.
42. Wen, C. and T. Chaung. Entrainment coal gasification modeling. in I & EC-Industrial and Engineering Chemistry, Process Design and Development, vol. 18, Oct. 1979, p. 684-695. 1979.
43. Vicente, W., et al., An Eulerian model for the simulation of an entrained flow coal gasifier. Applied Thermal Engineering, 2003. 23(15): p. 1993-2008.
44. Gerun, L., et al., Numerical investigation of the partial oxidation in a two-stage downdraft gasifier. Fuel, 2008. 87(7): p. 1383-1393.
45. Bouma, P., et al., Numerical modelling of an entrained-flow gasification simulator. ASME PRESSURE VESSELS PIPING DIV PUBL PVP, 1999. 397: p. 227-235.
46. Choi, Y.C., et al., Numerical study on the coal gasification characteristics in an entrained flow coal gasifier. Fuel, 2001. 80(15): p. 2193-2201.
47. Watanabe, H. and M. Otaka, Numerical simulation of coal gasification in entrained flow coal gasifier. Fuel, 2006. 85(12-13): p. 1935-1943.
48. Fletcher, D., et al., A CFD based combustion model of an entrained flow biomass gasifier. Applied mathematical modelling, 2000. 24(3): p. 165-182.
49. Ajilkumar, A., T. Sundararajan, and U.S.P. Shet, Numerical modeling of a steam-assisted tubular coal gasifier. International Journal of Thermal Sciences, 2009. 48(2): p. 308-321.
50. Silaen, A. and T. Wang, Investigation of the coal gasification process under various operating conditions inside a two-stage entrained flow gasifier. Journal of Thermal Science and Engineering Applications, 2012. 4(2): p. 021006.
51. Chui, E.H., et al., Simulation of entrained flow coal gasification. Energy Procedia, 2009. 1(1): p. 503-509.
52. Rajpar, S.A., To simulate the entrained flow gasifier for investigating its perofmance with various feed stocks, in Institute of Environmental Engineering & Managmenet. 2019, Mehran University of Engineering & Technology, Jamshoro.